

Beyond Low Rank + Sparse: Multi-scale Low Rank Matrix Decomposition

Frank Ong, and Michael Lustig

Department of Electrical Engineering and Computer Sciences

University of California, Berkeley

{frankong, mlustig}@eecs.berkeley.edu

Abstract

Low rank methods allow us to capture globally correlated components within matrices. The recent low rank + sparse decomposition further enables us to extract sparse entries along with the globally correlated components. In this paper, we present a natural generalization and consider the decomposition of matrices into components of multiple scales. Such decomposition is well motivated in practice as data matrices often exhibit local correlations in multiple scales. Concretely, we propose a multi-scale low rank modeling that represents a data matrix as a sum of block-wise low rank matrices with increasing scales of block sizes. We then consider the inverse problem of decomposing the data matrix into its multi-scale low rank components and approach the problem via a convex formulation. Theoretically, we show that under an incoherence condition, the convex program recovers the multi-scale low rank components exactly. Practically, we provide guidance on selecting the regularization parameters and incorporate cycle spinning to reduce blocking artifacts. Experimentally, we show that the multi-scale low rank decomposition provides a more intuitive decomposition than conventional low rank methods and demonstrate its effectiveness in four applications, including illumination normalization for face images, motion separation for surveillance videos, multi-scale modeling of the dynamic contrast enhanced magnetic resonance imaging and collaborative filtering exploiting age information.

Index Terms

Multi-scale Modeling, Low Rank Modeling, Convex Relaxation, Structured Matrix, Signal Decomposition

arXiv:1507.08751v2 [cs.LG] 4 Aug 2015

I. INTRODUCTION

Signals and systems often exhibit different structures at different scales. Such multi-scale structure has inspired a wide variety of multi-scale signal transforms, such as wavelets [1], curvelets [2] and multi-scale pyramids [3], that can represent natural signals compactly. Moreover, their ability to compress signal information into a few significant coefficients has made multi-scale signal transforms valuable beyond compression and are now commonly used in signal reconstruction applications, including denoising [4], compressed sensing [5], [6], and signal separation [7]–[9]. By now, multi-scale modeling is associated with many success stories in engineering applications.

On the other hand, multi-scale signal transforms, by design, require the input signals to lie on a predefined signal subspace. Hence, low rank methods are commonly used instead when the signal subspace needs to be estimated as well. In particular, low rank methods have seen great success in exploiting the global data correlation to recover the signal subspace and compactly represent the signal at the same time. Recent convex relaxation techniques [10] have further enabled low rank model to be adaptable to practical applications, including matrix completion [11], system identification [12] and phase retrieval [13], making low rank methods ever more attractive.

In this paper, we present a multi-scale low rank matrix decomposition method that incorporates multi-scale structures with low rank methods. The additional multi-scale structure allows us to obtain a more accurate and compact signal representation than conventional low rank methods whenever the signal exhibits multi-scale structures (see Figure 1). To capture data correlation at multiple scales, we model our data matrix as a sum of block-wise low rank matrices with increasing scales of block sizes (more detail in Section II) and consider the inverse problem of decomposing the matrix into its multi-scale components. Since we do not assume an explicit basis model, multi-scale low rank decomposition also prevents modeling errors or basis mismatch that are commonly seen with multi-scale signal transforms. In short, our proposed multi-scale low rank decomposition inherits the merits from both multi-scale modeling and low rank matrix decomposition.

Leveraging recent convex relaxation techniques, we propose a convex formulation to perform the multi-scale low rank matrix decomposition. We provide a theoretical analysis in Section IV that extends the rank-sparsity incoherence results in Chandrasekaran et al. [14]. We show that the proposed convex program can decompose the data matrix into its multi-scale components exactly, when the signal subspaces at each scale are sufficiently incoherent with other scales.

A major component of this paper is to introduce the proposed multi-scale low rank decomposition

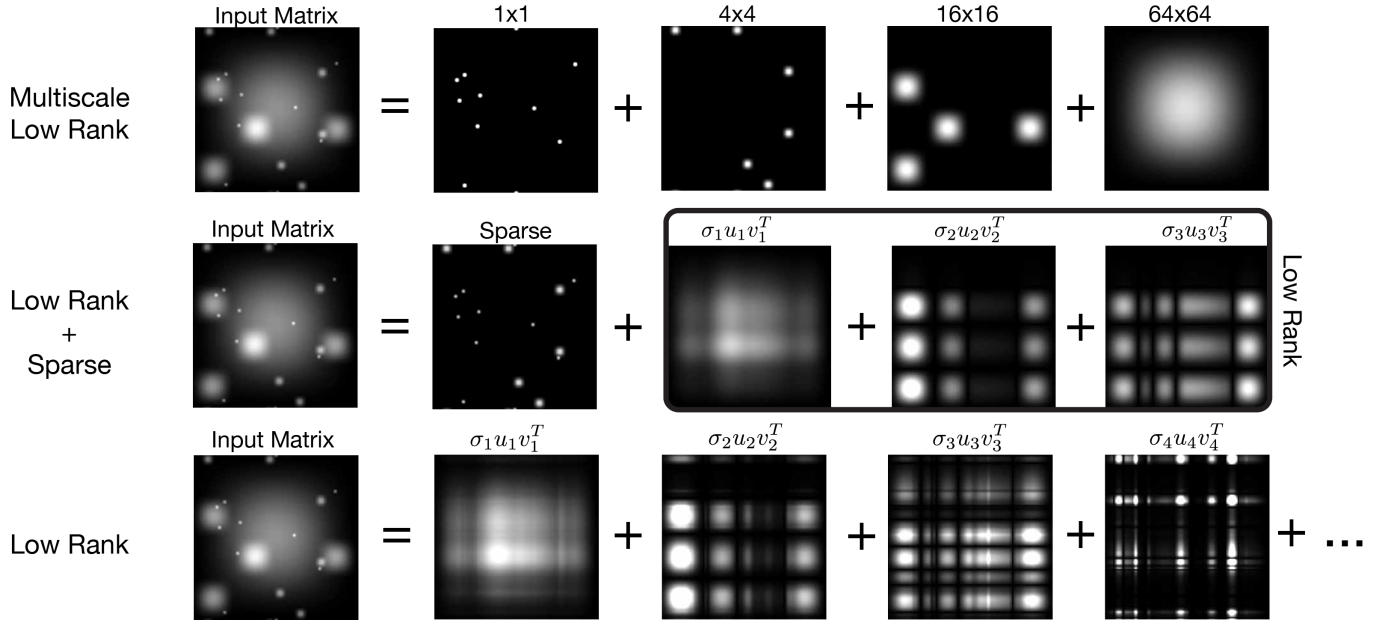


Fig. 1. An example of our proposed multi-scale low rank decomposition compared with other low rank methods. Each blob in the input matrix is a rank-1 matrix constructed from an outer product of hanning windows. Only the multi-scale low rank decomposition exactly separates the blobs to their corresponding scales and represents each blob as compactly as possible.

with emphasis on its practical performance and applications. We provide practical guidance on choosing regularization parameters for the convex method in Section VII and describe heuristics to perform cycle spinning [15] to reduce blocking artifacts in Section VIII. In addition, we applied the multi-scale low rank decomposition on real data and considered four applications of the multi-scale low rank decomposition: illumination normalization for face images, motion separation for surveillance videos, compact modeling of the dynamic contrast enhanced magnetic resonance imaging and collaborative filtering exploiting age information. (See Section IX for more detail). Our results show that the proposed multi-scale low rank decomposition provides intuitive multi-scale decomposition and compact signal representation for a wide range of applications.

Related work

Our proposed multi-scale low rank matrix decomposition draws many inspirations from recent developments in rank minimization [10], [11], [16]–[21]. In particular, the multi-scale low rank matrix decomposition is a generalization of the low rank + sparse decomposition proposed by Chandrasekaran et al. [14] and Candès et al. [22]. Our multi-scale low rank convex formulation also fits into the

convex demixing framework proposed by McCoy et al. [23]–[25], who studied the problem of demixing components from observation via convex optimization. The proposed multi-scale low rank decomposition can be viewed as a concrete and practical example of the convex demixing framework. Bakshi et al. [26] proposed a multi-scale principal component analysis by applying principal component analysis on wavelet transformed signals, but such method implicitly constrains the signal to lie on a predefined wavelet subspace. Various multi-resolution matrix factorization techniques [27], [28] were proposed to greedily peel off components of each scale by recursively applying matrix factorization. One disadvantage of these factorization methods is that it is not straightforward to incorporate them with other reconstruction problems as models.

II. MULTI-SCALE LOW RANK MATRIX MODELING

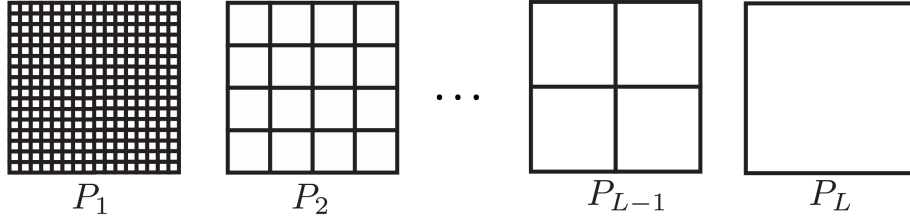
Low rank matrix modeling arises frequently in a wide variety of applications such as biomedical imaging [29], face recognition [30] and collaborative filtering [31]. In particular, when multiple copies of similar data $\{y_i\}_{i=1}^N$ are observed, the data matrix Y constructed as follows is often low rank:

$$Y = \begin{bmatrix} | & | & & | \\ y_1 & y_2 & \dots & y_N \\ | & | & & | \end{bmatrix} \quad (1)$$

While low rank modeling captures the notion of data similarity, it completely ignores any locality information that may be present in the data matrix. For example, in video processing, each data vector y_i represents a video frame and it is intuitive that each video frame should be more correlated with nearby frames than faraway frames. Hence the block matrix rank constructed from the data matrix is much lower than the global matrix rank. Such local low rank structure has been observed in various other applications, in particular in imaging applications [32]. Since natural data are naturally correlated in multiple scales, a multi-scale low rank modeling is intuitively a more appropriate modeling.

To concretely formulate the multi-scale low rank model, we assume that we can partition the data matrix Y into different scales. Specifically, we assume that we are given a multi-scale partition $\{P_i\}_{i=1}^L$ of the indices of an $M \times N$ matrix, where each block b in P_i is an order magnitude larger than the blocks in the previous scale P_{i-1} . Such multi-scale partition can be naturally obtained in many applications. For example in video processing, a multi-scale partition can be obtained by decimating both space and time dimensions. Figure 2 and 4 provide two examples of a multi-scale partition, the first one with decimation along two dimensions and the second one with decimation along one dimension. In Section IX, we provide practical examples on creating these multi-scale partitions for different applications.

Multi-scale Matrix Partition



Multi-scale Low Rank Modeling

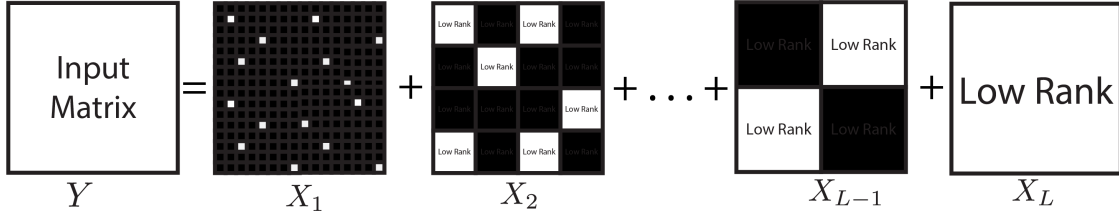


Fig. 2. Illustration of a multi-scale matrix partition and its associated multi-scale low rank modeling. Since the zero matrix is a matrix with the least rank, our multi-scale modeling naturally extends to sparse matrices as 1×1 low rank matrices.

To easily transform between the data matrix and the block matrices, we then consider a block reshape operator $R_b(X)$ that extracts a block b from the full matrix X and reshapes the block into an $m_i \times n_i$ matrix (Figure 3).

Block reshape operator

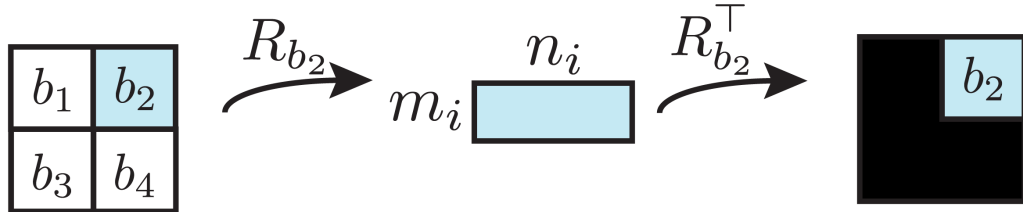


Fig. 3. Illustration of the block reshape operator R_b . R_b extracts block b from the full matrix and reshapes it into an $m_i \times n_i$ matrix. Its adjoint operator R_b^\top takes an $m_i \times n_i$ matrix and embeds it into a full-size zero matrix.

Given an $M \times N$ input matrix Y and its corresponding multi-scale partition and block reshape operators, we propose a multi-scale low rank modeling that models the $M \times N$ input matrix Y as a sum of matrices $\sum_{i=1}^L X_i$, in which each X_i is block-wise low rank with respect to its partition P_i . That is, we consider

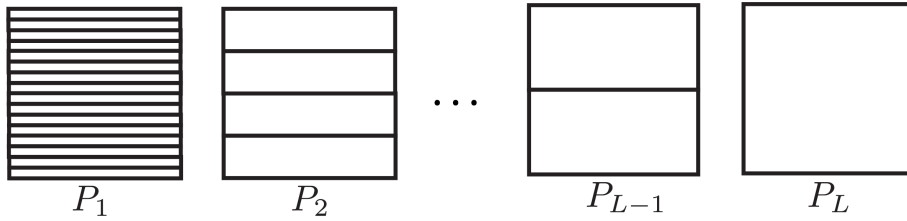
the following model for Y :

$$Y = \sum_{i=1}^L X_i \quad (2)$$

$$X_i = \sum_{b \in P_i} R_b^\top (U_b S_b V_b^\top)$$

where U_b , S_b , and V_b are matrices with sizes $m_i \times r_b$, $r_b \times r_b$ and $n_i \times r_b$ respectively and form the rank- r_b reduced SVD of $R_b(X_i)$. Note that when the rank of the block matrix $R_b(X_i)$ is zero, we have $\{U_b, S_b, V_b\}$ as empty matrices, which do not contribute to X_i . Figure 2 and 4 provide illustrations of two kinds of modeling with their associated partitions.

Multi-scale Matrix Partition



Multi-scale Low Rank Modeling

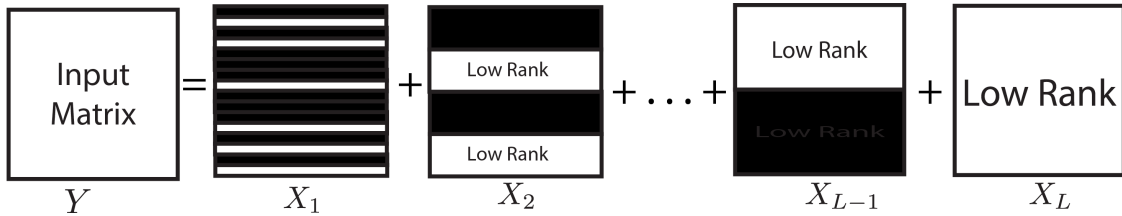


Fig. 4. Illustration of another multi-scale matrix partition and its associated multi-scale low rank modeling. Here, only the vertical dimension of the matrix is decimated. Since a $1 \times N$ matrix is low rank if and only if it is zero, our multi-scale modeling naturally extends to group sparse matrices.

By constraining each block matrices to be of low rank, the multi-scale low rank modeling captures the notion that nearby entries are more similar to each other than global entries in the data matrix. We note that the multi-scale low rank modeling is a generalization of the low rank + sparse modeling proposed by Chandrasekaren et al. [14] and Candès et al. [22]. In particular, the low rank + sparse modeling can be viewed as a 2-scale low rank modeling, in which the first scale has block size 1×1 and the second scale has block size $M \times N$. By adding additional scales between the sparse and globally low rank matrices, the multi-scale low rank modeling can capture locally low rank components that would otherwise need many coefficients to represent for low rank + sparse.

Given a data matrix Y that fits our multi-scale low rank model, our goal is to decompose the data matrix Y to its multi-scale components $\{X_i\}_{i=1}^L$. The ability to recover these multi-scale components is beneficial for many applications and allows us to, for example, extract motions at multiple scales in surveillance videos (Section IX). Since there are many more parameters to be estimated than the number of observations, it is necessary to impose conditions on X_i . In particular, we will exploit the fact that each block matrix is low rank via a convex program, which will be described in detail in section III.

Multi-scale low rank + noise

Before moving on to the convex formulation, we note that our multi-scale matrix decomposition can easily account for data matrices that are corrupted by additive white Gaussian noise. Under the multi-scale low rank modeling, we can think of the additive noise matrix as the largest scale signal component and is unstructured in any local scales. Specifically if we observe instead,

$$Y = \sum_{i=1}^L X_i + X_{\text{noise}} \quad (3)$$

where X_{noise} is an independent and identically distributed Gaussian noise matrix. Then we can define a reshape operator R_{noise} that reshapes the entire matrix into an $MN \times 1$ vector and the resulting matrix fits exactly to our multi-scale low rank model with $L+1$ scales. This incorporation of noise makes our model flexible in that it automatically provides a corresponding convex relaxation, a regularization parameter for the noise matrix and allows us to utilize the same iterative algorithm to solve for the noise matrix.

III. PROBLEM FORMULATION AND CONVEX RELAXATION

Given a data matrix Y that fits the multi-scale low rank model, our goal is to recover the underlying multi-scale components $\{X_i\}_{i=1}^L$ using the fact that X_i is block-wise low rank. Ideally, we would like to obtain a multi-scale decomposition with the minimal block matrix rank and solve a problem similar to the following form:

$$\begin{aligned} & \underset{X_1, \dots, X_L}{\text{minimize}} && \sum_{i=1}^L \sum_{b \in P_i} \text{rank}(R_b(X_i)) \\ & \text{subject to} && Y = \sum_{i=1}^L X_i \end{aligned} \quad (4)$$

However, to solve for the decomposition exactly seems hopeless in general as each rank minimization for each block is combinatorial in nature. In addition, it is not obvious whether the direct summation of ranks is a correct formulation as a 1-sparse matrix and a rank-1 matrix should intuitively not carry the

same cost. Hence, the above non-convex problem is not a practical formulation to obtain the multi-scale decomposition.

Fortunately, recent development in convex relaxations suggests that rank minimization problems can often be relaxed to a convex program via nuclear norm relaxation [10], [20], while still recovering the optimal solution to the original problem. In particular, Chandrasekaren et al. [14] and Candès et al., [22] showed that a low rank + sparse decomposition can be relaxed to a convex program by minimizing a nuclear norm + l_1 -norm objective as long as the signal constituents are incoherent with respect to each other. In addition, Candès et al., [22] showed that the regularization parameters for sparsity and low rank should be related by the square root of the matrix size. Hence, there is hope that, along the same line, we can perform the multi-scale low rank decomposition exactly via a convex formulation for certain matrices.

Concretely, let us define $\|\cdot\|_{\text{nuc}}$ to be the nuclear norm, the sum of singular values, and $\|\cdot\|_{\text{msv}}$ be the maximum singular value norm. For each scale i , we consider the block-wise nuclear norm to be the convex surrogate for the block-wise ranks. Specifically, we define $\|\cdot\|_{(i)}$ the block-wise nuclear norm for the i th scale as,

$$\|\cdot\|_{(i)} = \sum_{b \in P_i} \|R_b(\cdot)\|_{\text{nuc}} \quad (5)$$

It will also be useful to define its associated dual norm $\|\cdot\|_{(i)}^*$, which can be found as,

$$\|\cdot\|_{(i)}^* = \max_{b \in P_i} \|R_b(\cdot)\|_{\text{msv}} \quad (6)$$

which is the maximum of all block-wise maximum singular values.

We then consider the following convex relaxation for our multi-scale low rank decomposition problem:

$$\begin{aligned} & \underset{X_1, \dots, X_L}{\text{minimize}} && \sum_{i=1}^L \lambda_i \|X_i\|_{(i)} \\ & \text{subject to} && Y = \sum_{i=1}^L X_i \end{aligned} \quad (7)$$

where $\{\lambda_i\}_{i=1}^L$ are the regularization parameters and their selection will be described in detail in section VII.

Our convex formulation is a natural generalization of the low rank + sparse convex formulation [14], [22]. With the two sided matrix partition (Fig. 2), the nuclear norm applied to the 1×1 blocks becomes the element-wise l_1 -norm and the norm for the largest scale is the nuclear norm. With the one sided matrix partition (Fig. 4), the nuclear norm applied to $1 \times N$ blocks becomes the group-sparse norm and can be seen as a generalization of the group sparse + low rank decomposition [18]. If we incorporate

additive Gaussian noise in our model as mentioned above, then we have a nuclear norm applied to an $MN \times 1$ vector, which is equivalent to the Frobenius norm.

One should hope that the theoretical conditions from low rank + sparse can be generalized rather seamlessly to the multi-scale counterpart. Indeed, in the next section, we show that the core theoretical guarantees in Chandrasekaren et al. [14] for low rank + sparse can be generalized to the multi-scale setting. At a high level, we can show that as long as the row and column spaces of each block matrices are not coherent, then we can select appropriate regularization parameters $\{\lambda_i\}_{i=1}^L$ such that the resulting convex program recovers the multi-scale signal components $\{X_i\}_{i=1}^L$ from the data matrix Y .

Theoretical justification of the multi-scale low rank convex formulation can also be obtained via the convex demixing framework introduced in McCoy et al. [23]. In their work, McCoy et al. studied the problem of demixing signal constituents using a convex program and modeled the signal components to be randomly oriented with respect to each other. While real signal rarely have random components except noise and the random orientation assumption is not satisfied in our setting, McCoy et al. [23] provided strong guarantees on when the demixing succeeds and predicted a phase transition phenomenon. Since the multi-scale low rank decomposition fits the convex demixing framework, it also enjoys the same theoretical guarantees whenever the random orientation approximation is appropriate.

IV. THEORETICAL ASPECT OF THE MULTI-SCALE LOW RANK DECOMPOSITION

In this section, we provide theoretical justification of the proposed convex formulation and show that with a deterministic incoherence condition on $\{X_i\}_{i=1}^L$, the proposed convex formulation (7) recovers $\{X_i\}_{i=1}^L$ from Y exactly. If the reader is more interested in the practical aspect of the multi-scale low rank decomposition, he or she can skip to Section V.

Our proofs follow similar steps taken by Chandrasekaren et al. [14] on low rank + sparse decomposition and generalize them to the proposed multi-scale low rank decomposition. Our proof strategy is as follows: We first describe the subgradients of our objective function (Section IV-A) and define a coherence parameter in terms of the block-wise row and column spaces (Section IV-B). We then express an optimality condition of the convex program (7) in terms of a dual certificate. Finally, we show that with a deterministic condition on the coherence parameter, the optimality condition is satisfied and the optimal solution of the convex program is $\{X_i\}_{i=1}^L$ (Section IV-C).

A. Subdifferentials of the block-wise nuclear norms

To characterize the optimality of our convex problem, we first look at the subgradients of our objective function. We recall that for any matrix X with $\{U, S, V\}$ as its reduced SVD representation, the subdifferential of $\|\cdot\|_{\text{nuc}}$ at X is given by [20], [33],

$$\begin{aligned} \partial\|X\|_{\text{nuc}} = \{ & UV^\top + W : W \text{ and } X \text{ have orthogonal row} \\ & \text{and column spaces and } \|W\|_{\text{msv}} \leq 1\} \end{aligned} \quad (8)$$

Now recall that we define the block-wise nuclear norm to be $\|\cdot\|_{(i)} = \sum_{b \in P_i} \|R_b(\cdot)\|_{\text{nuc}}$. Then using the chain rule and the fact that $R_b(X_i) = U_b S_b V_b^\top$, we can obtain an expression for the subdifferential of $\|\cdot\|_{(i)}$ at X_i as follows:

$$\begin{aligned} \partial\|X_i\|_{(i)} = \{ & \sum_{b \in P_i} R_b^\top (U_b V_b^\top + W_b) : W_b \text{ and } R_b(X_i) \text{ have} \\ & \text{orthogonal row and column spaces and } \|W_b\|_{\text{msv}} \leq 1\} \end{aligned} \quad (9)$$

To simplify our notation, we define $E_i = \sum_{b \in P_i} R_b^\top (U_b V_b^\top)$ and T_i to be a vector space that contains matrices with the same block-wise row spaces or column spaces as X_i , that is,

$$T_i = \left\{ \sum_{b \in P_i} R_b^\top (U_b X_b^\top + Y_b V_b^\top) : X_b \in \mathbb{C}^{n_i \times r_i}, Y_b \in \mathbb{C}^{m_i \times r_i} \right\} \quad (10)$$

Then, the subdifferential of each $\|\cdot\|_{(i)}$ at X_i can be compactly represented as,

$$\partial\|X_i\|_{(i)} = \{E_i + W_i : W_i \in T_i^\perp \text{ and } \|W_i\|_{(i)}^* \leq 1\} \quad (11)$$

In the following of the section, we will be interested in projecting a matrix X onto T_i , which can be done with the following operation:

$$\begin{aligned} \mathcal{P}_{T_i}(X) = \sum_{b \in P_i} & R_b^\top (U_b U_b^\top R_b(X) + R_b(X) V_b V_b^\top \\ & - U_b U_b^\top R_b(X) V_b V_b^\top) \end{aligned} \quad (12)$$

Similarly, to project a matrix X onto the orthogonal complement of T_i , we can apply the following operation:

$$\mathcal{P}_{T_i^\perp}(X) = \sum_{b \in P_i} R_b^\top ((I - U_b U_b^\top) R_b(X) (I - V_b V_b^\top)) \quad (13)$$

where I is an appropriately sized identity matrix. Finally, we note that since $\|X\|_{(i)}^* = \max_{b \in P_i} \|R_b(X)\|_{\text{msv}}$, using the variational representation of the maximum singular value norm, we can show that for any matrix X , the following two inequalities hold,

$$\|\mathcal{P}_{T_i}(X)\|_{(i)}^* \leq \|X\|_{(i)}^* \quad (14)$$

$$\|\mathcal{P}_{T_i^\perp}(X)\|_{(i)}^* \leq \|X\|_{(i)}^* \quad (15)$$

B. Incoherence

Recent developments in signal processing suggests that exact signal decomposition can be achieved as long as the components are incoherent with respect to each other. Following Chandrasekaren et al. [14], we consider a deterministic measure of incoherence through the block-wise column and row spaces of X_i .

Formally, we define the coherence parameter for the j th scale signal component X_j with respect to the i th scale to be the following:

$$\mu_{ij} = \max_{N_j \in T_j, \|N_j\|_{(j)}^* \leq 1} \|N_j\|_{(i)}^* \quad (16)$$

Using μ_{ij} as a measure of incoherence, we can quantitatively say that the j th scale signal component is incoherent with respect to the i th scale if μ_{ij} is small. One property that we will frequently use is that for any $N_j \in T_j$ and $i \neq j$,

$$\|N_j\|_{(i)}^* \leq \mu_{ij} \|N_j\|_{(j)}^* \quad (17)$$

In the case of low rank + sparse, Chandrasekaren et al. [14] provides excellent descriptions of the concepts behind the coherence parameters. We refer the reader to their paper for the intuition behind these parameters.

The first result (Theorem IV.1) that we will show using the coherence parameters is that if we can choose some parameters to “balance” the coherence between the scales, then the block-wise row/column spaces $\{T_i\}_{i=1}^L$ are independent, that is $\sum_{i=1}^L T_i$ is a direct sum. Consequently, each matrix N in the span of $\{T_i\}_{i=1}^L$ has a unique decomposition $N = \sum_{i=1}^L N_i$, where $N_i \in T_i$.

Proposition IV.1. If we can choose some positive parameters $\{\lambda_i\}_{i=1}^L$ such that,

$$\sum_{j \neq i} \mu_{ij} \frac{\lambda_j}{\lambda_i} < 1, \quad \text{for } i = 1, \dots, L \quad (18)$$

then we have,

$$T_i \cap \sum_{j \neq i} T_j = \{0\}, \quad \text{for } i = 1, \dots, L \quad (19)$$

In particular when $L = 2$, the condition on $\{\mu_{12}, \mu_{21}\}$ reduces to $\mu_{12}\mu_{21} < 1$, which coincides with Proposition 1 in Chandrasekaren et al. [14]. We also note that given μ_{ij} , we can obtain $\{\lambda_i\}_{i=1}^L$ that satisfies the condition $\sum_{j \neq i} \mu_{ij} \lambda_j < \lambda_i$ by solving a linear program.

Proof. Suppose by contradiction that there exists $\{\lambda_i\}_{i=1}^L$ such that $\sum_{j \neq i} \mu_{ij} \lambda_j / \lambda_i < 1$, but $T_i \cap \sum_{j \neq i} T_j \neq \{0\}$. Then there exists $\{N_i \in T_i\}_{i=1}^L$ such that $\sum_{i=1}^L \lambda_i N_i = 0$ and not all N_i are zero.

But this leads to a contradiction because for $i = 1, \dots, L$,

$$\begin{aligned}
\|N_i\|_{(i)}^* &= \left\| - \sum_{j \neq i} \frac{\lambda_j}{\lambda_i} N_j \right\|_{(i)}^* \\
&\leq \sum_{j \neq i} \frac{\lambda_j}{\lambda_i} \mu_{ij} \|N_j\|_{(j)}^* \\
&\leq \left(\sum_{j \neq i} \frac{\lambda_j}{\lambda_i} \mu_{ij} \right) \max_{j \neq i} \|N_j\|_{(j)}^* \\
&< \max_{j \neq i} \|N_j\|_{(j)}^*
\end{aligned} \tag{20}$$

where we have used equation (17) for the first inequality and $\sum_{j \neq i} \mu_{ij} \lambda_j / \lambda_i < 1$ for the last inequality. \square

C. Theorems

In the following, we will show two theorems that lead to the conclusion that under a deterministic incoherence condition, the proposed convex program recovers $\{X_i\}_{i=1}^L$ from Y . Our proof makes use of the dual certificate proof techniques common in such proofs. Our first theorem shows an optimality condition of the convex program (7) in terms of its dual solution. Our second theorem shows that as long as we can balance the coherence parameters between scales with the regularization parameters $\{\lambda_i\}_{i=1}^L$, we can construct a dual solution that satisfies the optimality condition in the first theorem and thus $\{X_i\}_{i=1}^L$ is the unique optimizer of the proposed convex problem (7).

Theorem IV.2 (Lemma 4.2 [34]). $\{X_i\}_{i=1}^L$ is the unique minimizer of the convex program (7) if there exists a matrix Q such that for $i = 1, \dots, L$,

- 1) $\mathcal{P}_{T_i}(Q) = \lambda_i E_i$
- 2) $\|\mathcal{P}_{T_i^\perp} Q\|_{(i)}^* < \lambda_i$

Proof. Consider any non-zero perturbation $\{\Delta_i\}_{i=1}^L$ to $\{X_i\}_{i=1}^L$ such that $\{X_i + \Delta_i\}_{i=1}^L$ stays in the feasible set, that is $\sum_{i=1}^L \Delta_i = 0$. We will show that $\sum_{i=1}^L \lambda_i \|X_i + \Delta_i\|_{(i)} > \sum_{i=1}^L \lambda_i \|X_i\|_{(i)}$.

We first decompose Δ_i into orthogonal parts with respect to T_i , that is, $\Delta_i = \mathcal{P}_{T_i}(\Delta_i) + \mathcal{P}_{T_i^\perp}(\Delta_i)$. We also consider a specific subgradient $G = [G_1 \cdots G_L]^\top$ of $\sum_{i=1}^L \lambda_i \|\cdot\|_{(i)}$ at $\{X_i\}_{i=1}^L$ such that

$\|\mathcal{P}_{T_i^\perp}(G_i)\|_{(i)}^* \leq \lambda$, and $\langle \mathcal{P}_{T_i^\perp}(\Delta_i), \mathcal{P}_{T_i^\perp}(G_i) \rangle = \lambda_i \|\mathcal{P}_{T_i^\perp}(\Delta_i)\|_{(i)}$. Then, we have,

$$\begin{aligned}
\sum_{i=1}^L \lambda_i \|X_i + \Delta_i\|_{(i)} &\geq \sum_{i=1}^L \lambda_i \|X_i\|_{(i)} + \langle \Delta_i, G_i \rangle \\
&= \sum_{i=1}^L \lambda_i \|X_i\|_{(i)} + \langle \Delta_i, G_i \rangle - \langle \Delta_i, Q \rangle \\
&= \sum_{i=1}^L \lambda_i \|X_i\|_{(i)} + \langle \mathcal{P}_{T_i^\perp}(\Delta_i), \mathcal{P}_{T_i^\perp}(G_i) \rangle \\
&\quad - \langle \mathcal{P}_{T_i^\perp}(\Delta_i), \mathcal{P}_{T_i^\perp}(Q) \rangle \\
&\geq \sum_{i=1}^L \lambda_i \|X_i\|_{(i)} + \lambda_i \|\mathcal{P}_{T_i^\perp}(\Delta_i)\|_{(i)} \\
&\quad - \|\mathcal{P}_{T_i^\perp}(\Delta_i)\|_{(i)} \|\mathcal{P}_{T_i^\perp}(Q)\|_{(i)}^* \\
&> \sum_{i=1}^L \lambda_i \|X_i\|_{(i)}
\end{aligned} \tag{21}$$

where we obtained the first inequality from the definition of subgradient, and the first equality using $\sum_{i=1}^L \Delta_i = 0$.

□

Theorem IV.3. If we can choose regularization parameters $\{\lambda_i\}_{i=1}^L$ such that

$$\sum_{j \neq i} \mu_{ij} \frac{\lambda_j}{\lambda_i} < \frac{1}{2}, \quad \text{for } i = 1, \dots, L \tag{22}$$

then $\{X_i\}_{i=1}^L$ is the unique optimizer of the proposed convex problem (7).

In particular when the number of scales $L = 2$, the condition on $\{\mu_{12}, \mu_{21}\}$ reduces to $\mu_{12}\mu_{21} < 1/4$ and the condition on $\{\lambda_1, \lambda_2\}$ reduces to $2\mu_{12} < \lambda_1/\lambda_2 < 1/(2\mu_{21})$, which is in similar form as Theorem 2 in Chandrasekaran et al. [14].

Proof. Since $\sum_{j \neq i} \mu_{ij} \lambda_j / \lambda_i < 1/2$, by Proposition IV.1, $T_i \cap \sum_{j \neq i} T_j = \{0\}$ for all i . Thus, there is a unique matrix Q in $\sum_{i=1}^L T_i$ such that $\mathcal{P}_{T_i}(Q) = \lambda_i E_i$. In addition, Q can be uniquely expressed as a sum of elements in T_i . That is, $Q = \sum_{i=1}^L Q_i$ with $Q_i \in T_i$. We now have a matrix Q that satisfies the first optimality condition. In the following, we will show that it also satisfies the second optimality condition $\|\mathcal{P}_{T_i^\perp} Q\|_{(i)}^* < \lambda_i$.

If the vector spaces $\{T_i\}_{i=1}^L$ are orthogonal, then Q_i is exactly $\lambda_i E_i$. Because they are not necessarily orthogonal, we can express Q_i as $\lambda_i E_i$ plus a correction term $\lambda_i \epsilon_i$. That is, we express $Q_i = \lambda_i (E_i + \epsilon_i)$.

Putting Q_i 's back to Q , we have,

$$Q = \sum_{i=1}^L \lambda_i (E_i + \epsilon_i) \quad (23)$$

From the first optimality condition $\mathcal{P}_{T_i}(Q) = \lambda_i E_i$ and using equation (23), we can obtain the following recursive expression for ϵ_i :

$$\epsilon_i = -\mathcal{P}_{T_i} \left(\sum_{j \neq i} \frac{\lambda_j}{\lambda_i} (E_j + \epsilon_j) \right) \quad (24)$$

We can now obtain a bound on $\|\mathcal{P}_{T_i^\perp}(Q)\|_{(i)}^*$ in terms of ϵ_i ,

$$\begin{aligned} \|\mathcal{P}_{T_i^\perp}(Q)\|_{(i)}^* &= \|\mathcal{P}_{T_i^\perp} \left(\sum_{j \neq i} \lambda_j (E_j + \epsilon_j) \right)\|_{(i)}^* \\ &\leq \left\| \sum_{j \neq i} \lambda_j (E_j + \epsilon_j) \right\|_{(i)}^* \\ &\leq \sum_{j \neq i} \mu_{ij} \lambda_j (1 + \|\epsilon_j\|_{(j)}^*) \\ &\leq \left(\sum_{j \neq i} \mu_{ij} \lambda_j \right) \max_{j \neq i} (1 + \|\epsilon_j\|_{(j)}^*) \end{aligned} \quad (25)$$

The first inequality is due to equation (15) and the second one from the property of incoherence (17) and triangle inequality.

Similarly, we can obtain a recursive expression for $1 + \|\epsilon_i\|_{(i)}^*$ using equation (24),

$$\begin{aligned} 1 + \|\epsilon_i\|_{(i)}^* &= 1 + \left\| \mathcal{P}_{T_i} \left(\sum_{j \neq i} \frac{\lambda_j}{\lambda_i} (E_j + \epsilon_j) \right) \right\|_{(i)}^* \\ &\leq 1 + \left\| \sum_{j \neq i} \frac{\lambda_j}{\lambda_i} (E_j + \epsilon_j) \right\|_{(i)}^* \\ &\leq 1 + \sum_{j \neq i} \mu_{ij} \frac{\lambda_j}{\lambda_i} (1 + \|\epsilon_j\|_{(j)}^*) \\ &\leq 1 + \left(\sum_{j \neq i} \mu_{ij} \frac{\lambda_j}{\lambda_i} \right) \max_{j \neq i} (1 + \|\epsilon_j\|_{(j)}^*) \end{aligned} \quad (26)$$

Taking the maximum over i on both sides and rearranging, we have,

$$\max_i (1 + \|\epsilon_i\|_{(i)}^*) \leq \frac{1}{1 - \max_i \sum_{j \neq i} \mu_{ij} \frac{\lambda_j}{\lambda_i}} \quad (27)$$

Putting the bound back to equation (25), we have,

$$\begin{aligned} \|\mathcal{P}_{T_i^\perp}(Q)\|_{(i)}^* &\leq \lambda_i \frac{\sum_{j \neq i} \mu_{ij} \frac{\lambda_j}{\lambda_i}}{1 - \max_i \sum_{j \neq i} \mu_{ij} \frac{\lambda_j}{\lambda_i}} \\ &< \lambda_i \end{aligned} \quad (28)$$

where we used $\sum_{j \neq i} \mu_{ij} \lambda_j / \lambda_i < 1/2$ in the last inequality.

Thus, we have constructed a dual certificate Q that satisfies the optimality conditions (21) and $\{X_i\}_{i=1}^L$ is the unique optimizer of the convex problem (7).

□

V. AN ITERATIVE ALGORITHM FOR SOLVING THE MULTI-SCALE LOW RANK DECOMPOSITION

In the following, we will derive an iterative algorithm that solves for the multi-scale low rank decomposition via the Alternating Direction of Multiple Multipliers (ADMM) [35]. While the proposed convex formulation (7) can be formulated into a semi-definite program, first-order iterative methods are commonly used when solving for large datasets for their computational efficiency and scalability. Moreover, iterative algorithms often provide practical insights to the convex problem itself. For multi-scale low rank decomposition, our iterative algorithm has the interpretation of repeatedly removing inter-scale interference on the observed data via thresholding the singular values as shown in Figure 5.

To formally obtain update steps using ADMM, we first formulate the problem into the standard ADMM form with two separable objectives connected by an equality constraint,

$$\begin{aligned} \underset{X_i, Z_i}{\text{minimize}} \quad & \mathbb{1}\{Y = \sum_{i=1}^L X_i\} + \sum_{i=1}^L \lambda_i \|Z_i\|_{(i)} \\ \text{subject to} \quad & X_i = Z_i \end{aligned} \quad (29)$$

where $\mathbb{1}\{\cdot\}$ is the indicator function.

To proceed, we then need to obtain the proximal operators [36] for the two objective functions $\mathbb{1}\{Y = \sum_{i=1}^L X_i\}$ and $\sum_{i=1}^L \lambda_i \|Z_i\|_{(i)}$. For the data consistency objective $\mathbb{1}\{Y = \sum_{i=1}^L X_i\}$, the proximal operator is simply the projection operator to the set. To obtain the proximal operator for the multi-scale nuclear norm objective $\sum_{i=1}^L \lambda_i \|X_i\|_{(i)}$, we first recall that the proximal operator for the nuclear norm $\|X\|_{\text{nuc}}$ with parameter λ is given by the singular value soft-threshold operator [20],

$$\text{SVT}_\lambda(X) = U \max(\Sigma - \lambda, 0) V^\top \quad (30)$$

Since we defined the block-wise nuclear norm for each scale i as $\sum_{b \in P_i} \|R_b(\cdot)\|_{\text{nuc}}$, the norm is separable with respect to each block and its proximal function with parameter λ_i is given by the block-wise singular value soft-threshold operator,

$$\text{BLOCKSVT}_{\lambda_i}(X) = \sum_{b \in P_i} R_b^\top(\text{SVT}_{\lambda_i}(R_b(X))) \quad (31)$$

which simply extracts every blocks in the matrix, performs singular value thresholding and puts the blocks back to the matrix. We note that for 1×1 blocks, the block-wise singular value soft-threshold

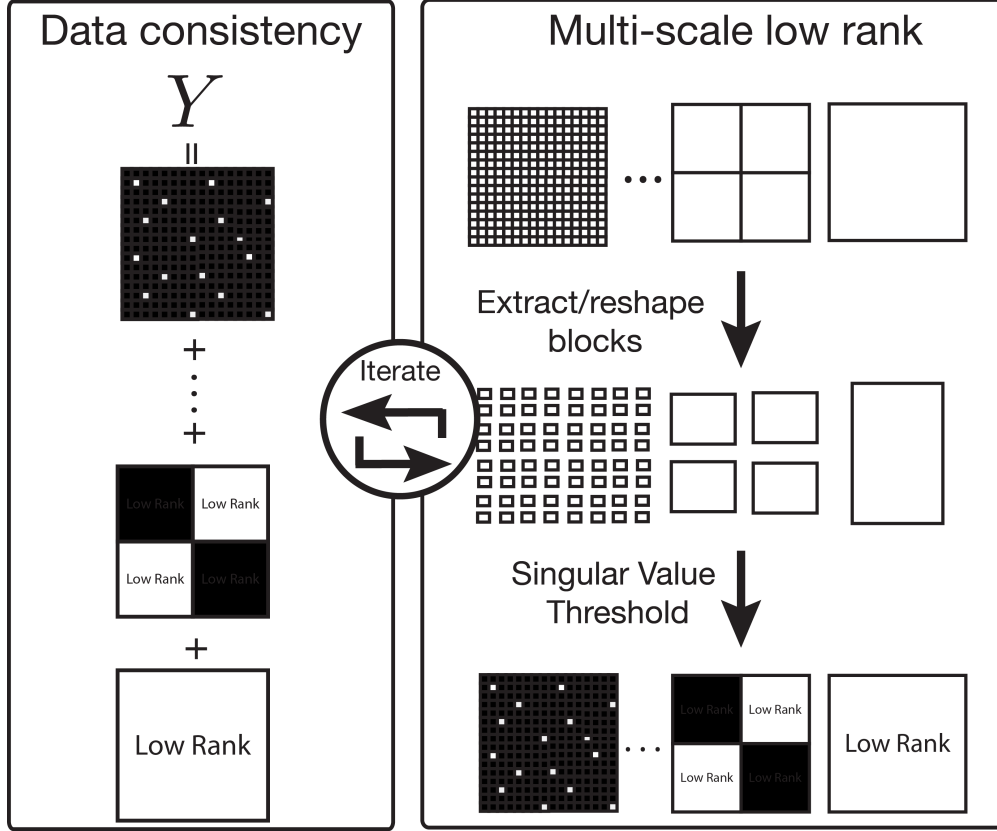


Fig. 5. A conceptual illustration of how to obtain a multi-scale low rank decomposition. First, we extract each block from the input matrix and perform a thresholding operation on its singular value to recover the significant components. Then, we subtract these significant components from our input matrix, thereby enabling the recovery of weaker, previously submerged components.

operator reduces to the element-wise soft-threshold operator and for $1 \times N$ blocks, the block-wise singular soft-threshold operator reduces to the joint soft-threshold operator.

Putting everything together and invoking the ADMM recipe [35], we have the following algorithm to solve our convex multi-scale low rank decomposition (7):

$$\begin{aligned}
 X_i &\leftarrow (Z_i - U_i) + \frac{1}{L} \left(Y - \sum_{i=1}^L (Z_i - U_i) \right) \\
 Z_i &\leftarrow \text{BLOCKSVT}_{\lambda_i/\rho}(X_i + U_i) \\
 U_i &\leftarrow U_i - (Z_i - X_i)
 \end{aligned} \tag{32}$$

where ρ is the ADMM parameter that only affects the convergence rate of the algorithm.

Indeed, the resulting ADMM update steps are similar in essence to the intuitive update steps in Figure 5,

and alternates between data consistency and enforcing multi-scale low rank. The major difference of ADMM is that it adds a dual update step with U_i , which bridges the two objectives and ensures the convergence to the optimal solution. Under the guarantees of ADMM, in the limit of iterations, X_i and Z_i converge to the optimal solution of the convex program (7) and U_i converges to a scaled version of the dual variable. In practice, we found that ~ 1000 iterations are sufficient without any visible change for imaging applications.

VI. COMPUTATIONAL COMPLEXITY

Given the iterative algorithm (32), one concern about the multi-scale low rank decomposition might be that it is significantly more computationally intensive than other low rank methods as we have many more SVD's and variables to compute for. In this section, we show that because we decimate the matrices at each scale geometrically, the theoretical computational complexity of the multi-scale low rank decomposition is similar to other low rank decomposition methods, such as the low rank + sparse decomposition.

For concreteness, let us consider the multi-scale partition with two-sided decimation shown in Figure 2 and have block sizes $m_i = 2^{i-1}$ and $n_i = 2^{i-1}$. Similar to other low rank methods, the SVD's dominate the per iteration complexity for the multi-scale low rank decomposition and has complexity $O(M \times N \text{ SVD}) = O(MN^2)$. The per iteration complexity for the multi-scale low rank decomposition is the summation of all the SVD's performed for each scale, which is given by,

$$\begin{aligned} & O(M \times N \text{ SVD}) + 4 O\left(\frac{M}{2} \times \frac{N}{2} \text{ SVD}\right) \\ & + 16 O\left(\frac{M}{4} \times \frac{N}{4} \text{ SVD}\right) + 64 O\left(\frac{M}{8} \times \frac{N}{8} \text{ SVD}\right) + \dots \\ & \leq \mathbf{2O}(M \times N \text{ SVD}) \end{aligned} \tag{33}$$

Hence, the computational complexity with the two-sided decimated partition is at most twice the computational complexity for a $M \times N$ matrix SVD. In general, one can show that the per-iteration complexity for arbitrary multi-scale partition is at most $\log(N)$ times the full matrix SVD, which is tolerable if a multi-scale modeling is more suitable modeling.

While theoretically, the computation cost for small block sizes should be less than bigger block sizes, we found that in practice the computation cost for computing the small SVD's can dominate the per-iteration computation. This is due to the overhead of copying small block matrices and calling library functions repeatedly to compute the SVD's.

Since we are interested in thresholding the singular values and in practice many of the small block matrices are zero as shown in Section IX, one trick of reducing the computation time is to quickly compute

an upper bound on the maximum singular value for block matrices before the SVD's. Then if the upper bound for the maximum singular value is less than the threshold, we know the thresholded matrix will be zero and can avoid computing the SVD at all. Since for any matrix X , its maximum singular value is bounded by the square root of any matrix norm on $X^\top X$ [37], there are many different upper bounds that we can use. In particular, we choose the maximum row norm and consider the following upper bound,

$$\sigma_{\max}(X) \leq \sqrt{\max_i \sum_j |X_{ik} X_{jk}|} \quad (34)$$

Using this upper bound, we can identify many below-the-threshold matrices before computing the SVD's at all. In practice, we found that the above trick provides a modest speedup of $3 \sim 5\times$.

VII. GUIDANCE ON CHOOSING REGULARIZATION PARAMETERS

In this section, we provide guidance on selecting the regularization parameters $\{\lambda_i\}_{i=1}^L$. Selecting the regularization parameters $\{\lambda_i\}_{i=1}^L$ is crucial for the convex decomposition to succeed, both theoretically and practically. While theoretically we can establish a criterion on selecting the regularization parameters (see Section IV), such parameters are not straightforward to calculate in practice as it requires the knowledge of the row and column space for each block matrix *before* the decomposition.

To select the regularization parameters $\{\lambda_i\}_{i=1}^L$, we follow the suggestions from Wright et al. [34] and Fogel et al. [38], and set each regularization parameter λ_i to be the Gaussian complexity of each norm $\|\cdot\|_{(i)}$, which is defined as the expectation of the dual norm of random Gaussian matrix:

$$\lambda_i \sim E[\|G\|_{(i)}^*] \quad (35)$$

where G is a unit-variance independent and identically distributed random Gaussian matrix.

The resulting expression for the Gaussian complexity is the maximum singular value of a random Gaussian matrix, which has been studied extensively in Bandeira et al. [39]. The recommended regularization parameter for scale i can be found as,

$$\lambda_i \sim \sqrt{m_i} + \sqrt{n_i} + \sqrt{\log\left(\frac{MN}{\max\{m_i, n_i\}}\right)} \quad (36)$$

For the sparse matrix scale with 1×1 block size, $\lambda_i \sim \sqrt{\log(MN)}$ and for the globally low rank scale with $M \times N$ block size, $\lambda_i \sim \sqrt{M} + \sqrt{N}$. Hence this regularization parameter selection is consistent with the ones recommended for low rank + sparse decomposition by Candès et al. [22]. In addition, for the noise matrix with $MN \times 1$ block size, $\lambda_i \sim \sqrt{MN}$, which has similar scaling as in square root

lasso [40]. In practice, we found that the suggested regularization parameter selection allows exact multi-scale decomposition when the signal model is matched (for example Figure 1) and provides visually intuitive decomposition for real datasets.

One explanation for the above selection of the regularization parameters can be seen from the iterative procedure described in the Section V. As described in the iterative algorithm, the regularization parameters are the thresholds that are chosen to suppress interference from other scales. Now consider the special case that our input matrix Y is a random Gaussian matrix. Then in order to have exact recovery, we would want to have all multi-scale components $\{X_i\}_{i=1}^L$ to be zero except the one that represents the noise matrix. Hence, each threshold or regularization parameter, should be chosen such that it is greater than all the block-wise singular values of the Gaussian matrix. That is,

$$\lambda_i \geq \max_{b \in P_i} \|R_b(G)\|_{\text{msv}} \quad (37)$$

which is simply the dual norm of the Gaussian matrix. By results in concentration inequalities, we know that choosing λ_i to be the expectation of the dual norm guarantees that the inequality is satisfied with high probability.

VIII. HEURISTICS FOR TRANSLATIONAL INVARIANT DECOMPOSITION

Similar to wavelet transforms, one drawback of the multi-scale low rank decomposition is that it is not translational invariant. In practice, this translational variant nature often creates blocking artifacts near the block boundaries, which can be visually jarring for image or video applications. One solution to remove these artifacts is to introduce overlapping partitions of the matrix so that the overall algorithm is translational invariant. However, this vastly increases both memory and computation especially for large block sizes. In the following, we will describe a cycle spinning approach that we used in practice to reduce the blocking artifacts with only slight increase in per-iteration computation.

Cycle spinning [15] has been commonly used in wavelet denoising to reduce the blocking artifacts due to the translational variant nature of the wavelet transform. To minimize artifacts, cycle spinning averages the denoised results from all possible shifts, thereby making the entire process translational invariant. In words cycle spinning for wavelet denoising can be described as,

$$\text{AVERAGE[SHIFT - DENOISE - UNSHIFT]} \quad (38)$$

In the context of multi-scale low rank decomposition, we can make the iterative algorithm translational invariant by replacing the block-wise singular value thresholding operation in each iteration with its cycle

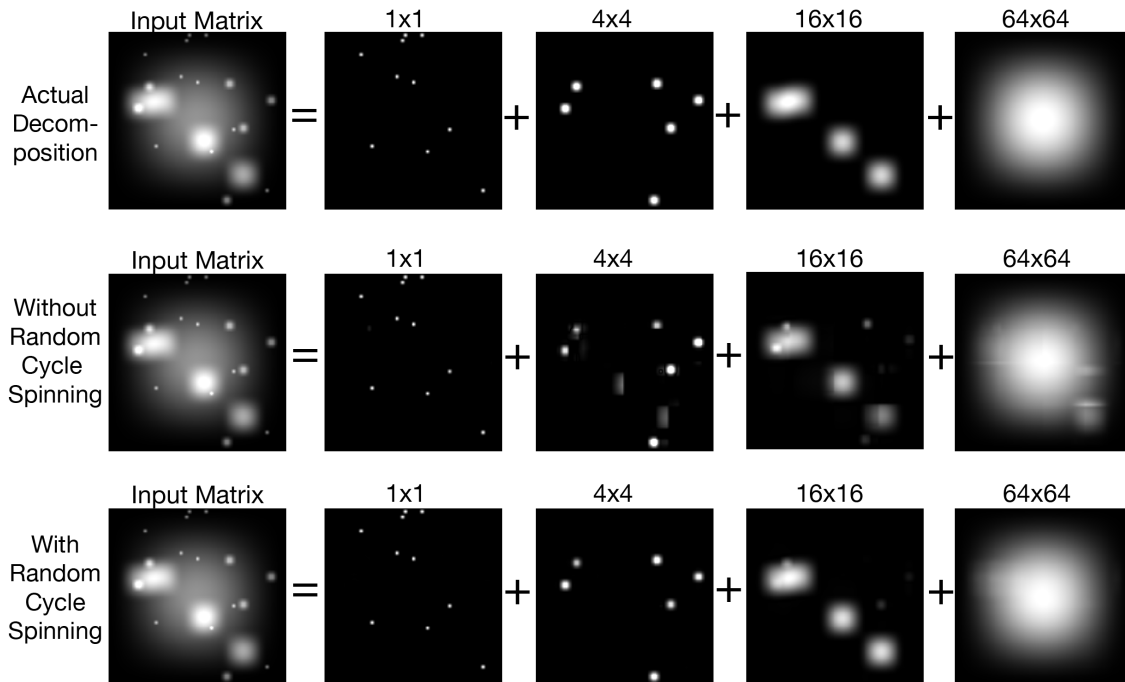


Fig. 6. An example of the multi-scale low rank decomposition with and without random cycle spinning. Each blob in the input matrix Y is a rank-1 matrix constructed from an outer product of hanning windows and is placed at random positions. Blocking artifacts can be seen in the decomposition without random cycle spinning while vastly diminished in the random cycle spinned decomposition.

spinning counterpart, that is,

$$\text{AVERAGE}[\text{SHIFT} - \text{BLOCKSVT} - \text{UNSHIFT}] \quad (39)$$

To further reduce computation, we can perform random cycle spinning in each iteration as described in Figueiredo et al. [41], in which we randomly shifts the input, performs block-wise singular value thresholding and then unshifts back:

$$\text{RANDOMSHIFT} - \text{BLOCKSVT} - \text{RANDOMUNSHIFT} \quad (40)$$

Using random cycle spinning, blocking artifacts caused by thresholding are averaged over iterations and in practice, reduces distortion significantly. Figure 6 shows an example of the multi-scale low rank decomposition with and without random cycle spinning applied on a simulated data that does not fall on the partition grid. The decomposition with random cycle spinning vastly reduces blocking artifacts that appeared in the one without random cycle spinning.

IX. APPLICATIONS

To test for practical performance, we applied the multi-scale low rank decomposition on four different real datasets that are conventionally used in low rank modeling: illumination normalization for face images (Section IX-A), motion separation for surveillance videos (Section IX-B), multi-scale modeling of dynamic contrast enhanced magnetic resonance imaging (Section IX-C) and collaborative filtering exploiting age information (Section IX-D). We compared our proposed multi-scale low rank decomposition with low rank + sparse decomposition for the first three applications and with low rank matrix completion for the last application. Randomly cycle spinning was used for multi-scale low rank decomposition for all of our experiments. Regularization parameters λ_i were chosen exactly as $\sqrt{m_i} + \sqrt{n_i} + \sqrt{\log(\frac{MN}{\max\{m_i, n_i\}})}$ for multi-scale low rank and $\max(m_i, n_i)$ for low rank + sparse decomposition. Our simulations were written in the C programming language and ran on a 20-core Intel Xeon workstation. Some results are best viewed in video format, which are available as supplementary materials.

In the spirit of reproducible research, we provide a software package (in C and partially in MATLAB) to reproduce most of the results described in this paper. The software package can be downloaded from:

<http://www.eecs.berkeley.edu/~mlustig/Software.html>

A. Multi-scale Illumination Normalization for Face Recognition Pre-processing

Face recognition algorithms are sensitive to shadows or occlusions on faces. In order to obtain the best possible performance for these algorithms, it is desired to remove illumination variations and shadows on the face images. Low rank modeling are often used to model faces and is justified by approximating faces as convex Lambertian surfaces [30].

Low rank + sparse decomposition [22] was recently proposed to capture uneven illumination as sparse errors and was shown to remove small shadows while capturing the underlying faces as the low rank component. However, most shadows are not sparse and contain structure over different lighting conditions. Here, we propose modeling shadows and illumination changes in different face images as block-low rank as illumination variations are spatially correlated in multiple scales.

We considered face images from the Yale B face database [42]. Each face image was of size 192×168 with 64 different lighting conditions. The images were then reshaped into a $32,256 \times 64$ matrix and both multi-scale low rank and low rank + sparse decomposition were applied on the data matrix. For low rank + sparse decomposition, we found that the best separation result was obtained when each face image was normalized to the maximum value. For multi-scale low rank decomposition, the original unscaled image

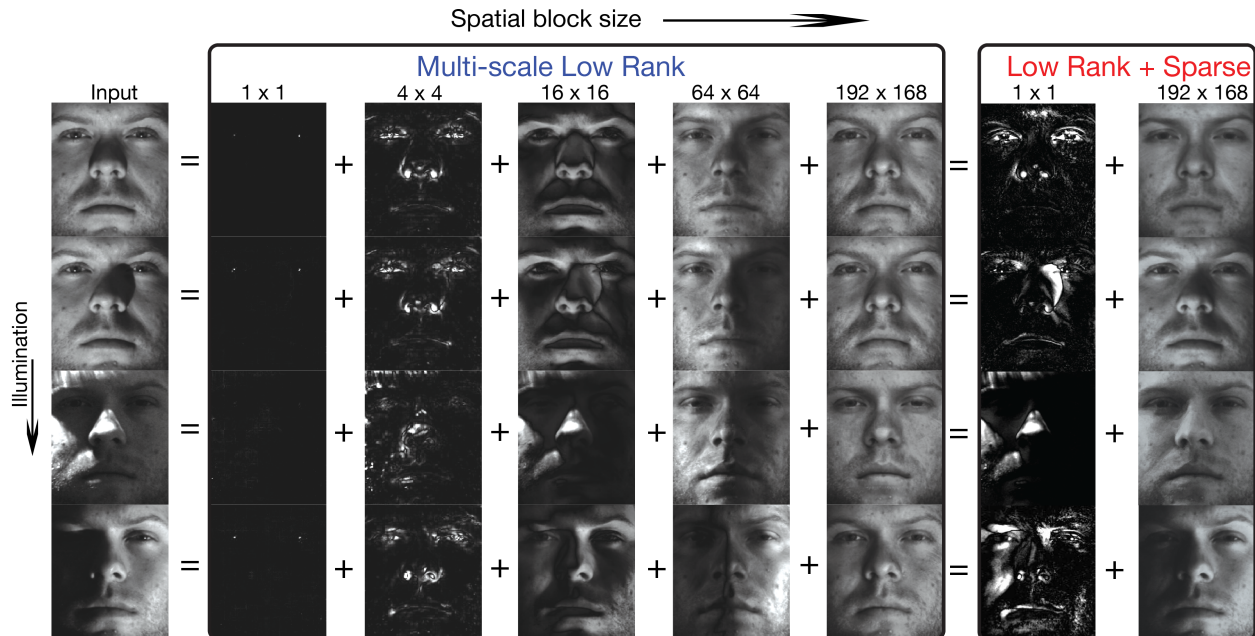


Fig. 7. Multi-scale low rank versus low rank + sparse on faces with uneven illumination. Multi-scale low rank decomposition recovers almost shadow-free faces, whereas low rank + sparse decomposition can only remove some shadows.

was used. Only the space dimension was decimated as we assumed there was no ordering in different illumination conditions. The multi-scale matrix partition can be visualized as in Figure 4.

Figure 7 shows one of the comparison results. Multi-scale low rank decomposition recovered almost shadow-free faces. In particular, the sparkles in the eyes were represented in the 1×1 block size and the larger illumination changes were represented in bigger blocks, thus capturing most of the uneven illumination changes. In contrast, low rank + sparse decomposition could only recover from small illumination changes and still contained the larger shadows in the globally low rank component.

B. Multi-scale Motion Separation for Surveillance Videos

In surveillance video processing, it is desired to extract foreground objects from the video. To be able to extract foreground objects, both the background and the foreground dynamics have to be modeled. Low rank modeling have been shown to be suitable for slowly varying videos, such as background illumination changes. In particular, if the video background only changes its brightness over time, then it can be represented as a rank-1 matrix.

Low rank + sparse decomposition [22] was proposed to foreground objects as sparse components and

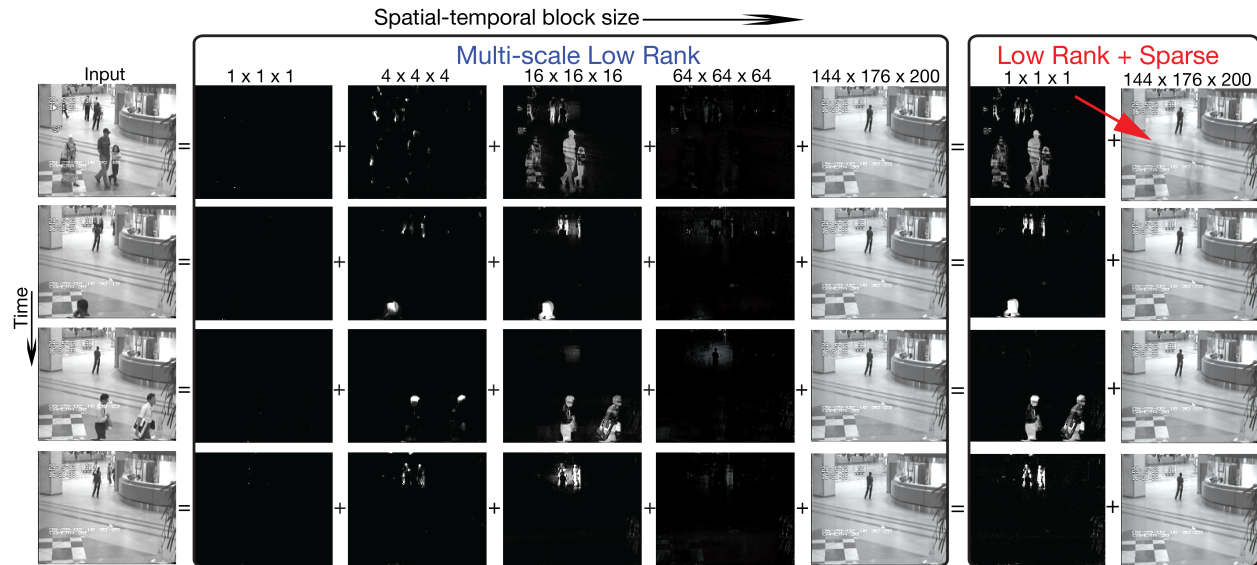


Fig. 8. Multi-scale low rank versus low rank + sparse decomposition on a surveillance video. For the multi-scale low rank, body motion is mostly captured in the $16 \times 16 \times 16$ scale while fine-scale motion is captured in $4 \times 4 \times 4$ scale. Background video component is captured in the globally low rank component and is almost artifact-free. Low rank + sparse decomposition exhibits ghosting artifacts as pointed by the red arrow because they are neither globally low rank or sparse.

was shown to separate dynamics from background components. However, sparsity alone cannot capture motion compactly and often results in ghosting artifacts occurring around the foreground objects as shown in Figure 8. Since video dynamics are correlated locally at multiple scales in space and time, we propose using the multi-scale low rank modeling with two sided decimation to capture different scales of video dynamics over space and time.

We considered a surveillance video from Li et al. [43]. Each video frame was of size 144×176 and the first 200 frames were used. The video frames were then reshaped into a $25,344 \times 200$ matrix and both multi-scale low rank and low rank + sparse decomposition were applied on the data matrix.

Figure 8 shows one of the results. Multi-scale low rank decomposition recovered a mostly artifact free background video in the globally low rank component whereas low rank + sparse decomposition exhibits ghosting artifact in certain segments of the video. For the multi-scale low rank decomposition, body motion was mostly captured in the $16 \times 16 \times 16$ scale while fine-scale motion was captured in $4 \times 4 \times 4$ scale.

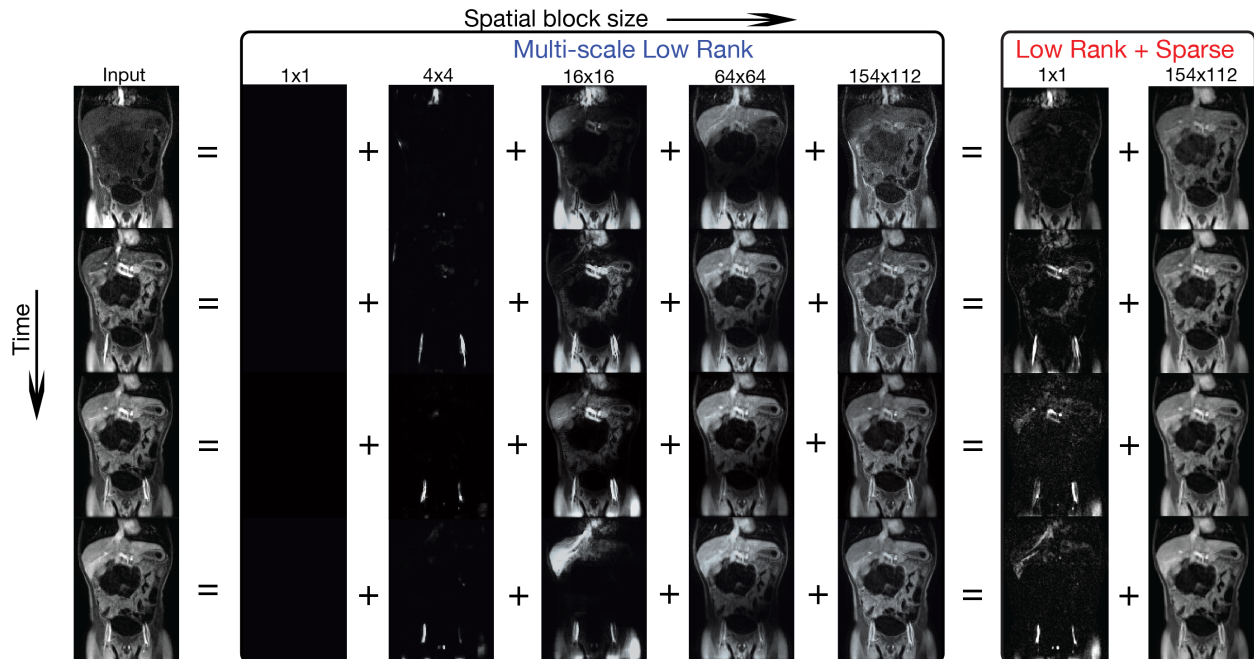


Fig. 9. Multi-scale low rank versus low rank + sparse decomposition on a dynamic contrast enhanced magnetic resonance image series. For the multi-scale result, small contrast dynamics in vessels are captured in 4×4 blocks while contrast dynamics in the liver are captured in 16×16 blocks. The biggest block size captures the static tissues and interestingly the respiratory motion. In contrast, the low rank + sparse modeling could only provide a coarse separation of dynamics and static tissue, which result in neither truly sparse nor truly low rank components.

C. Multi-scale Low Rank Modeling for Dynamic Contrast Enhanced Magnetic Resonance Imaging

In dynamic contrast enhanced magnetic resonance imaging (DCE-MRI), a series of images over time is acquired after a T_1 contrast agent was injected into the patient. Different tissues then exhibit different contrast dynamics over time, thereby allowing radiologists to characterize and examine lesions. Compressed sensing Magnetic Resonance Imaging [44] is now a popular research approach used in three dimensional DCE-MRI to speed up acquisition. Since the more compact we can represent the image series, the better our compressed reconstruction result becomes, an accurate modeling of the dynamic image series is desired to improve the compressed sensing reconstruction results for DCE-MRI.

When a region contains only one type of tissue, then the block matrix constructed by stacking each frame as columns will have rank 1. Hence, low rank modeling [29], and locally low rank modeling [45] have been popular models for DCE-MRI. Recently, low rank + sparse modeling [46] have also been proposed to model the static background and dynamics as low rank and sparse matrices respectively.

However, dynamics in DCE-MRI are almost never sparse and often exhibit correlation across different scales. Hence, we propose using a multi-scale low rank modeling to capture contrast dynamics over multiple scales.

We considered a fully sampled dynamic contrast enhanced image data. The data was acquired in a pediatric patient with 20 contrast phases, $1 \times 1.4 \times 2 \text{ mm}^3$ resolution, and 8s temporal resolution. The acquisition was performed on a 3T GE MR750 scanner with a 32-channel cardiac array using an RF-spoiled gradient-echo sequence. We considered a 2D slice of size 154×112 were then reshaped into a $17,248 \times 20$ matrix. Both multi-scale low rank and low rank + sparse decomposition were applied on the data matrix.

Figure 9 shows one of the results. In the multi-scale low rank decomposition result, small contrast dynamics in vessels were captured in 4×4 blocks while contrast dynamics in the liver were captured in 16×16 blocks. The biggest block size captured the static tissues and interestingly the respiratory motion. Hence, different types of contrast dynamics were captured compactly in their suitable scales. In contrast, the low rank + sparse modeling could only provide a coarse separation of dynamics and static tissue, which resulted in neither truly sparse nor truly low rank components.

D. Multi-scale Age Grouping for Collaborative Filtering

Collaborative filtering is the task of making predictions about the interests of a user using available information from all users. Since users often have similar taste for the same item, low rank modeling is commonly used to exploit the data similarity to complete the rating matrix [11], [19], [20]. On the other hand, low rank matrix completion does not exploit the fact that users with similar demographic backgrounds have similar taste for similar items. In particular, users of similar age should have similar taste. Hence, we incorporated the proposed multi-scale low rank modeling with matrix completion by partitioning users according to their age and compared it with the conventional low rank matrix completion.

To incorporate multi-scale low rank modeling into matrix completion, we change the data consistency constraint in problem (7) to $[Y]_{jk} = [\sum_{i=1}^L X_i]_{jk}$ for observed jk entries, and correspondingly, the update step for $\{X_i\}_{i=1}^L$ in equation (32) is changed to $[X_i]_{jk} \leftarrow [(Z_l - U_i) + \frac{1}{L}(Y - \sum_{i=1}^L (Z_i - U_i))]_{jk}$ for observed jk entries and $[X_i]_{jk} \leftarrow [Z_l - U_i]_{jk}$ for unobserved jk entries.

To compare the methods, we considered the 100K MovieLens dataset, in which 943 users rated 1682 movies. The resulting matrix was of size 1682×943 , where the first dimension represented movies and the second dimension represented users. The entire matrix had 93.7% missing entries. Test data was

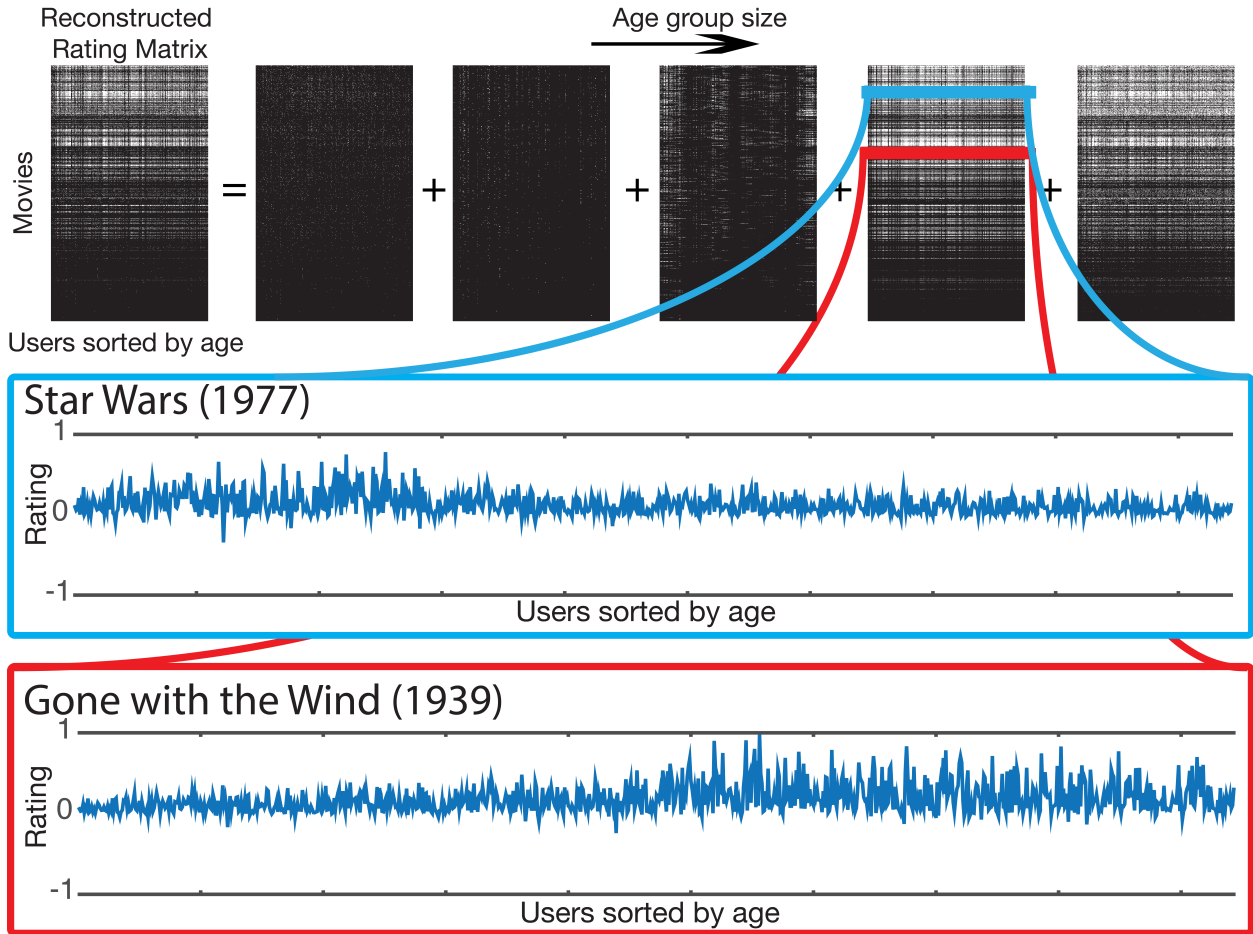


Fig. 10. Multi-scale low rank reconstructed matrix of the 100K MovieLens dataset. The extracted signal scale component captures the tendency that younger users rated Star Wars higher whereas the more senior users rated Gone with the Wind higher.

further generated by randomly undersampling the rating matrix by 5. The algorithms were then run on the test data and root mean squared errors were calculated over all available entries. To obtain a multi-scale partition of the matrix, we sorted the users according to their age along the second dimension and partitioned them evenly into age groups.

Figure 10 shows a multi-scale low rank reconstructed user rating matrix. Using multiple scales of block-wise low rank matrices, correlations in different age groups were captured. For example, one of the scales shown in Figure 10 captures the tendency that younger users rated Star Wars higher whereas the more senior users rated Gone with the Wind higher. The multi-scale low rank reconstructed matrix achieved a root mean-squared-error of 0.9385 compared to a root mean-squared-error of 0.9552 for the

low rank reconstructed matrix.

X. DISCUSSION

We have presented a multi-scale low rank matrix decomposition method that combines both multi-scale modeling and low rank matrix decomposition. Using a convex formulation, we can solve for the decomposition efficiently and exactly, provided that the multi-scale signal components are incoherent. We provided a theoretical analysis of the convex relaxation, which extends from the analysis in Chandrasekaran et al. [14], and provided empirical evidence that the multi-scale low rank decomposition performs well on real datasets.

We would also like to emphasize that the multi-scale low rank decomposition does not have any free parameter if the recommended regularization parameters are used, which empirically performed well even with the addition of noise. Hence, the multi-scale low rank prevents manual tuning and works “right-out-of-the-box”. On the other hand, theoretical guarantees for the regularization parameters are not provided and would be valuable for future work.

Our experiments show that the multi-scale low rank decomposition improves upon the low rank + sparse decomposition in a variety of applications. On the other hand, we believe that more improvement can be achieved if domain knowledge for each applications is incorporated with the multi-scale low rank decomposition. For example, for movie rating collaborative filtering, general demographic information and movie types can be used to construct multi-scale partitions in addition to age information. For face shadow removal, prior knowledge of the illumination angle might be able to provide a better multi-scale partition.

REFERENCES

- [1] S. G. Mallat, “A theory for multiresolution signal decomposition: the wavelet representation,” *Pattern Analysis and Machine Intelligence*, 1989. [Online]. Available: http://ieeexplore.ieee.org/xpls/abs_all.jsp?arnumber=192463
- [2] E. Candes, L. Demanet, D. Donoho, and L. Ying, “Fast discrete curvelet transforms,” *Multiscale Modeling & Simulation*, 2006. [Online]. Available: <http://epubs.siam.org/doi/abs/10.1137/05064182X>
- [3] E. P. Simoncelli, W. T. Freeman, E. H. Adelson, and D. J. Heeger, “Shiftable multiscale transforms,” *Information Theory, IEEE Transactions on*, vol. 38, no. 2, pp. 587–607, Mar. 1992. [Online]. Available: <http://ieeexplore.ieee.org/lpdocs/epic03/wrapper.htm?arnumber=119725>
- [4] D. L. Donoho and I. M. Johnstone, “Ideal spatial adaptation by wavelet shrinkage,” *Biometrika*, vol. 81, no. 3, pp. 1–31, Sep. 2006. [Online]. Available: <http://www.jstor.org/stable/2337118?origin=crossref>
- [5] D. L. Donoho, “Compressed sensing,” *Information Theory, IEEE Transactions on*, vol. 52, no. 4, pp. 1289–1306, Apr. 2006. [Online]. Available: <http://ieeexplore.ieee.org/lpdocs/epic03/wrapper.htm?arnumber=1614066>

- [6] E. J. Candes, J. Romberg, and T. Tao, “Robust uncertainty principles: exact signal reconstruction from highly incomplete frequency information,” *Information Theory, IEEE Transactions on*, vol. 52, no. 2, pp. 489–509, 2006. [Online]. Available: <http://ieeexplore.ieee.org/lpdocs/epic03/wrapper.htm?arnumber=1580791>
- [7] D. L. Donoho and X. Huo, “Uncertainty principles and ideal atomic decomposition,” *Information Theory, IEEE Transactions on*, vol. 47, no. 7, pp. 2845–2862, Nov. 2001. [Online]. Available: <http://ieeexplore.ieee.org/lpdocs/epic03/wrapper.htm?arnumber=959265>
- [8] J. L. Starck, Y. Moudden, J. Bobin, M. Elad, and D. L. Donoho, “Morphological component analysis,” *Optics & Photonics 2005*, vol. 5914, pp. 59 140Q–59 140Q–15, Aug. 2005. [Online]. Available: <http://proceedings.spiedigitallibrary.org/proceeding.aspx?articleid=870615>
- [9] S. S. Chen, D. L. Donoho, and M. A. Saunders, “Atomic decomposition by basis pursuit,” *SIAM Journal on Scientific Computing*, vol. 20, no. 1, pp. 33–61, 1998. [Online]. Available: <http://epubs.siam.org/doi/abs/10.1137/S1064827596304010>
- [10] M. Fazel, “Matrix rank minimization with applications,” Ph.D. dissertation, Stanford University, Mar. 2002. [Online]. Available: <https://faculty.washington.edu/mfazel/thesis-final.pdf>
- [11] E. J. Candès and B. Recht, “Exact Matrix Completion via Convex Optimization,” *Foundations of Computational Mathematics*, vol. 9, no. 6, pp. 717–772, Dec. 2009. [Online]. Available: <http://link.springer.com/10.1007/s10208-009-9045-5>
- [12] M. Fazel, T. K. Pong, D. Sun, and P. Tseng, “Hankel Matrix Rank Minimization with Applications to System Identification and Realization,” *SIAM Journal on Matrix Analysis and Applications*, vol. 34, no. 3, pp. 946–977, Jul. 2013. [Online]. Available: <http://epubs.siam.org/doi/abs/10.1137/110853996>
- [13] E. J. Candès, Y. C. Eldar, T. Strohmer, and V. Voroninski, “Phase Retrieval via Matrix Completion,” *SIAM Journal on Imaging Sciences*, vol. 6, no. 1, pp. 199–225, Feb. 2013. [Online]. Available: <http://epubs.siam.org/doi/abs/10.1137/110848074>
- [14] V. Chandrasekaran, S. Sanghavi, and P. A. Parrilo, “Rank-sparsity incoherence for matrix decomposition,” *SIAM Journal on ...*, 2011. [Online]. Available: <http://epubs.siam.org/doi/abs/10.1137/090761793>
- [15] R. R. Coifman and D. L. Donoho, “Translation-Invariant De-Noising,” in *Wavelets and Statistics*. New York, NY: Springer New York, 1995, pp. 125–150. [Online]. Available: http://link.springer.com/10.1007/978-1-4612-2544-7_9
- [16] B. Recht, W. Xu, and B. Hassibi, “Null space conditions and thresholds for rank minimization,” *Mathematical Programming*, vol. 127, no. 1, pp. 175–202, Oct. 2010. [Online]. Available: <http://link.springer.com/10.1007/s10107-010-0422-2>
- [17] A. Agarwal, S. Negahban, and M. J. Wainwright, “Noisy matrix decomposition via convex relaxation: Optimal rates in high dimensions,” *The Annals of Statistics*, vol. 40, no. 2, pp. 1171–1197, Apr. 2012. [Online]. Available: <http://projecteuclid.org/euclid.aos/1342625465>
- [18] H. Xu, C. Caramanis, and S. Sanghavi, “Robust PCA via outlier pursuit,” *Advances in Neural Information ...*, pp. 2496–2504, 2010. [Online]. Available: <http://papers.nips.cc/paper/4005-robust-pca-via-outlier-pursuit>
- [19] E. J. Candes and T. Tao, “The Power of Convex Relaxation: Near-Optimal Matrix Completion,” *Information Theory, IEEE Transactions on*, vol. 56, no. 5, pp. 2053–2080, May 2010. [Online]. Available: <http://ieeexplore.ieee.org/lpdocs/epic03/wrapper.htm?arnumber=5452187>
- [20] B. Recht, M. Fazel, and P. A. Parrilo, “Guaranteed Minimum-Rank Solutions of Linear Matrix Equations via Nuclear Norm Minimization,” *dx.doi.org*, vol. 52, no. 3, pp. 471–501, Aug. 2010. [Online]. Available: <http://epubs.siam.org/doi/abs/10.1137/070697835>
- [21] D. Hsu, S. M. Kakade, and T. Zhang, “Robust Matrix Decomposition With Sparse Corruptions,” *Information Theory*,

- IEEE Transactions on*, vol. 57, no. 11, pp. 7221–7234, 2011. [Online]. Available: <http://ieeexplore.ieee.org/lpdocs/epic03/wrapper.htm?arnumber=5934412>
- [22] E. J. Candès, X. Li, Y. Ma, and J. Wright, “Robust principal component analysis?” *Journal of the ACM*, vol. 58, no. 3, pp. 1–37, May 2011. [Online]. Available: <http://portal.acm.org/citation.cfm?doid=1970392.1970395>
- [23] M. B. McCoy and J. A. Tropp, “The achievable performance of convex demixing,” *arXiv.org*, Sep. 2013. [Online]. Available: <http://arxiv.org/abs/1309.7478v1>
- [24] —, “Sharp recovery bounds for convex demixing, with applications,” *Foundations of Computational Mathematics*, vol. 14, no. 3, pp. 1–51, Jan. 2014. [Online]. Available: <http://link.springer.com/10.1007/s10208-014-9191-2>
- [25] M. B. McCoy, V. Cevher, Q. T. Dinh, and A. Asaei, “Convexity in source separation: Models, geometry, and algorithms,” *IEEE Signal Processing Magazine*, vol. 31, no. 3, pp. 87–95, 2014. [Online]. Available: http://ieeexplore.ieee.org/xpls/abs_all.jsp?arnumber=6784106
- [26] B. R. Bakshi, “Multiscale PCA with application to multivariate statistical process monitoring,” *AIChE Journal*, vol. 44, no. 7, pp. 1596–1610, Jul. 1998. [Online]. Available: <http://doi.wiley.com/10.1002/aic.690440712>
- [27] R. Kondor, N. Teneva, and V. Garg, “Multiresolution Matrix Factorization,” in *The 31st International Conference on Machine Learning*, 2014, pp. 1620–1628. [Online]. Available: <http://jmlr.org/proceedings/papers/v32/kondor14.html>
- [28] R. Kakarala and P. O. Ogunbona, “Signal analysis using a multiresolution form of the singular value decomposition,” *Image Processing*, 2001. [Online]. Available: http://ieeexplore.ieee.org/xpls/abs_all.jsp?arnumber=918566
- [29] Z. P. Liang, “Spatiotemporal imaging with partially separable functions,” in *Biomedical Imaging: From Nano to Macro*. IEEE, 2007, pp. 988–991. [Online]. Available: <http://ieeexplore.ieee.org/lpdocs/epic03/wrapper.htm?arnumber=4193454>
- [30] R. Basri and D. W. Jacobs, “Lambertian reflectance and linear subspaces,” *IEEE Transactions on Pattern Analysis and Machine Intelligence*, vol. 25, no. 2, pp. 218–233, Feb. 2003. [Online]. Available: <http://ieeexplore.ieee.org/lpdocs/epic03/wrapper.htm?arnumber=1177153>
- [31] K. Goldberg, T. Roeder, D. Gupta, and C. Perkins, “Eigentaste: A Constant Time Collaborative Filtering Algorithm,” *Information Retrieval*, vol. 4, no. 2, pp. 133–151, 2001. [Online]. Available: <http://link.springer.com/10.1023/A:1011419012209>
- [32] J. Trzasko, A. Manduca, and E. Borisch, “Local versus global low-rank promotion in dynamic MRI series reconstruction,” *Proc Int Symp Magn Reson . . .*, 2011. [Online]. Available: <http://cds.ismrm.org/protected/11MProceedings/files/4371.pdf>
- [33] G. A. Watson, “Characterization of the subdifferential of some matrix norms,” *Linear Algebra and Its Applications*, 1992. [Online]. Available: <http://www.sciencedirect.com/science/article/pii/0024379592904072>
- [34] J. Wright, A. Ganesh, K. Min, and Y. Ma, “Compressive principal component pursuit,” *Information and Inference: A Journal of the IMA*, 2013. [Online]. Available: <http://imaia.oxfordjournals.org/content/2/1/32.short>
- [35] S. Boyd, “Distributed Optimization and Statistical Learning via the Alternating Direction Method of Multipliers,” *Foundations and Trends® in Machine Learning*, vol. 3, no. 1, pp. 1–122, 2010. [Online]. Available: https://web.stanford.edu/~boyd/papers/pdf/admm_distr_stats.pdf
- [36] N. Parikh and S. Boyd, “Proximal algorithms,” *Foundations and Trends in optimization*, 2013. [Online]. Available: http://web.stanford.edu/~boyd/papers/pdf/prox_algs.pdf
- [37] R. A. Horn and C. R. Johnson, *Matrix Analysis*. Cambridge University Press, Oct. 2012. [Online]. Available: <https://books.google.com/books?id=5I5AYeeh0JUC>
- [38] R. Foygel and L. Mackey, “Corrupted sensing: Novel guarantees for separating structured signals,” *Information Theory*, vol. 60, no. 2, pp. 1223–1247, 2014. [Online]. Available: http://ieeexplore.ieee.org/xpls/abs_all.jsp?arnumber=6712045

- [39] A. S. Bandeira and R. van Handel, “Sharp nonasymptotic bounds on the norm of random matrices with independent entries,” *arXiv.org*, Aug. 2014. [Online]. Available: <http://arxiv.org/abs/1408.6185v3>
- [40] A. Belloni, V. Chernozhukov, and L. Wang, “Square-root lasso: pivotal recovery of sparse signals via conic programming,” *Biometrika*, 2011. [Online]. Available: <http://biomet.oxfordjournals.org/content/98/4/791.short>
- [41] M. A. T. Figueiredo and R. D. Nowak, “An EM algorithm for wavelet-based image restoration,” *IEEE Transactions on Image Processing*, vol. 12, no. 8, pp. 906–916, Aug. 2003. [Online]. Available: <http://ieeexplore.ieee.org/lpdocs/epic03/wrapper.htm?arnumber=1217267>
- [42] A. S. Georghiades, P. N. Belhumeur, and D. J. Kriegman, “From few to many: illumination cone models for face recognition under variable lighting and pose,” *IEEE Transactions on Pattern Analysis and Machine Intelligence*, vol. 23, no. 6, pp. 643–660, 2001. [Online]. Available: <http://ieeexplore.ieee.org/lpdocs/epic03/wrapper.htm?arnumber=927464>
- [43] L. Li, W. Huang, I. Y. H. Gu, and Q. Tian, “Statistical Modeling of Complex Backgrounds for Foreground Object Detection,” *IEEE Transactions on Image Processing*, vol. 13, no. 11, pp. 1459–1472, Nov. 2004. [Online]. Available: <http://ieeexplore.ieee.org/lpdocs/epic03/wrapper.htm?arnumber=1344037>
- [44] M. Lustig, D. Donoho, and J. M. Pauly, “Sparse MRI: The application of compressed sensing for rapid MR imaging,” *Magnetic Resonance in Medicine*, vol. 58, no. 6, pp. 1182–1195, 2007. [Online]. Available: <http://doi.wiley.com/10.1002/mrm.21391>
- [45] T. Zhang, J. Y. Cheng, A. G. Potnick, R. A. Barth, M. T. Alley, M. Uecker, M. Lustig, J. M. Pauly, and S. S. Vasanawala, “Fast pediatric 3D free-breathing abdominal dynamic contrast enhanced MRI with high spatiotemporal resolution,” *Journal of Magnetic Resonance Imaging*, vol. 41, no. 2, pp. 460–473, Feb. 2015. [Online]. Available: <http://doi.wiley.com/10.1002/jmri.24551>
- [46] R. Otazo, E. Candès, and D. K. Sodickson, “Low-rank plus sparse matrix decomposition for accelerated dynamic MRI with separation of background and dynamic components,” *Magnetic Resonance in Medicine*, pp. n/a–n/a, Apr. 2014. [Online]. Available: <http://doi.wiley.com/10.1002/mrm.25240>